Journal of Computational Acoustics,

INVERSION OF PRESSURE DATA ON A VERTICAL ARRAY FOR SEAFLOOR GEOACOUSTIC PROPERTIES

PURNIMA RATILAL
DSO National Laboratories, 20 Science Park Drive, Singapore 118230

PETER GERSTOFT
Marine Physical Laboratory, Scripps Institute of Oceanography
University of California, San Diego, CA 92093-0701

JOO THIAM GOH and KENG PONG YEO
DSO National Laboratories, 20 Science Park Drive, Singapore 118230

Received (to be inserted
Revised by Publisher)

Estimation of the integral geoacoustic properties of the sea floor based on real data drawn from a shallow water site is presented. Two independent inversion schemes are used to deduce these properties. The first is matched field processing of the pressure field on a vertical line array due to a projected source. The second approach is the inversion of ambient noise on a vertical array. Matched field processing has shown success in the inversion of high quality field data. Here, we show that it is also feasible with a more practical and less expensive data collection scheme. It will also be shown that low frequency inversion is more robust to variation and fluctuation in the propagating medium, whereas high frequencies are more sensitive to mismatches in a varying medium. A comparison is made of the estimates obtained from the two techniques and also with available historical data of the trial site.

1. Introduction

In underwater applications, Matched Field Processing (MFP)[1,2] has been used as an inverse method for source localization as well as obtaining information about the environment. It involves measuring the acoustic field usually on a vertical array of receivers with the source at a fixed distance from the array. The unknown properties of the environment are determined from the measured field by matching the acoustic field patterns with a forward propagation model. These forward models require information about the environment and the geometries of the measurement as inputs. Multiple iterations of the forward model are performed as a function of the unknown parameters over a given search space. This optimization is often done with either simulated annealing[3] or genetic algorithms[4]. The parameter set that gives the highest correlation of the forward model predictions to the measured data is taken as the solution.

Matched field processing has been shown to be successful in the inversion of high quality data obtained from well-controlled experiments[5]. In these experiments, physical knowledge of the environment and *a priori* information have been systematically exploited to eliminate from the inverse problem the need to infer volume and bottom structures, and experimental geometries that are known or directly measurable. The instrumentation employed in the acquisition of these data is extensive. It includes an array that spans a significant proportion of the water column and is bottom moored to avoid drifting. The array has sufficient number of receivers to sample the wavefield at the desired frequencies. Array positioning systems using transponders are deployed to ensure accurate knowledge of hydrophone positioning. Low frequencies are extensivly used in these measurements and subsequently, in the inversion. This *a priori* knowledge of the geometric and geoacoustic properties of the experiment is often coupled into the parameterization to ensure that meaningful estimates are obtained. Less perfect vertical arrays have also been used. Michalopoulou *et al.*[6] used data from 5 hydrophones covering about 22 m in the analysis of time series in order to estimate geometric parameters. Chapman *et al.*[7,8] used a 10 hydrophone 40-m array in deep water to estimate geoacoustic properties using an adaptive simulated annealing method[9] for data at single frequencies in the range 10–20 Hz.

Practical data collection schemes on the other hand, do not have the luxury of extensive equipment set-up or measurement time. Little *a priori* information would be available and practical systems always have to contend with a higher rate of equipment failure. A question arises as to whether meaningful inversion may result from such measurements. Our studies show that inversion is still possible under certain circumstances. There are two essential factors to consider. Firstly the limitation of the measurement system has to be understood and subsequently incorporated in the processing. Secondly, an understanding of the interaction of acoustic fields with the environment should be used in the parameterization of the environment especially where *a priori* information is lacking.

In September 1996, a shallow water experiment was conducted with the aim of collecting data to study inverse methods currently in use to determine the geoacoustic properties of the sea bottom. Data for the matched field inversion were collected using a simple measurement set-up consisting of an array and a source deployed from freely drifting vessels. We had little *a priori* information about the trial site.

Where inversion for the properties of the sea bottom is concerned, results of MFP are often compared to information about the sea bottom obtained from cores[5,10]. This leads to some difficulties due to the fact that cores provide estimates of the sea bottom properties at the specific points where they are extracted. Moreover, there is a limit to the number of cores that can be extracted. MFP on the other hand provides estimates of these properties integrated over the measurement range. The estimates obtained from MFP reflect the overall effect of the bottom as compared to a single point measurement. During our experiment, the ambient noise at the trial location was measured and these data were inverted to estimate the properties of the sea bottom. In ambient noise inversion (ANI) the features of the ambient noise field are matched to a model of the noise field based on some physical environment[11]. It is a MFP technique that uses the naturally occurring ambient noise in

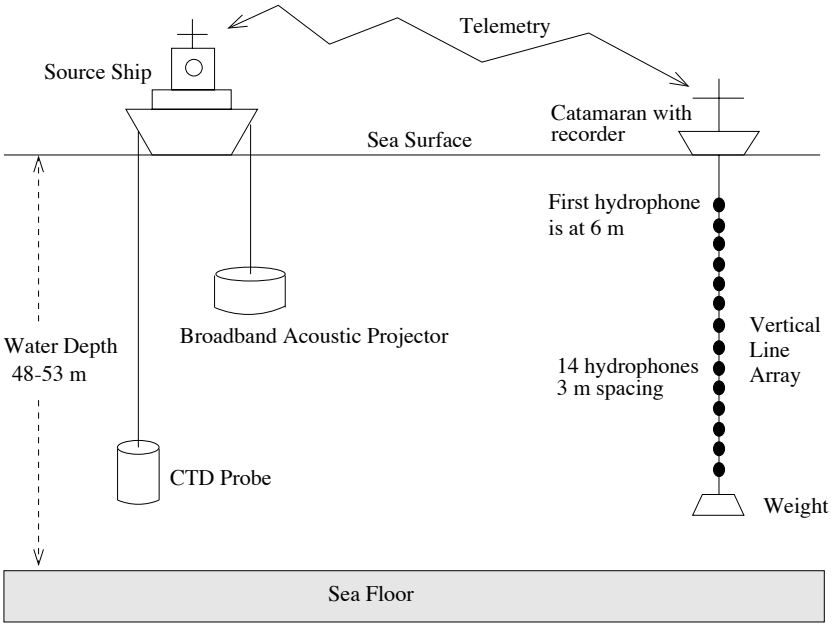

Figure 1: Experimental Setup

the sea to provide the source of acoustic field needed in the inversion.

Following this introduction, a detailed description of the experiment and data collected will be given. The processing methods implemented for inversion by the two approaches will be described and the results obtained are compared. Reference will also be made to available historical data of the trial site.

2. Experimental Data Collection

The experimental site has a fairly constant water depth over a large area, varying from 48 to 53 m. Figure 1 shows the experimental set-up during the trial.

The source used was a projector that was lowered to a water depth of approximately 14 m from the water surface. The projector was operated at various frequencies from 100 Hz to 2 kHz sequentially with each frequency of transmission being approximately 15 s in duration. The strength of the projected signal was 175 dB from 700 Hz to 2 kHz and 160 dB for frequencies below 700 Hz. The receiving Vertical Line Array (VLA) had 14 hydrophones with an inter-element spacing of 3 m. The first hydrophone was at a depth of approximately 6 m and the VLA spanned about 40 m of the water column. The array was attached to a battery powered catamaran in a free-floating configuration. Data on the array was recorded onto an analog recorder which was housed in the catamaran. Control of the recorder in the catamaran from the source ship was achieved through telemetry. The telemetry was also used to monitor the position of the catamaran which had a GPS receiver. The source ship was equipped with DGPS. The maximum error in our measurement of the separation between the source ship and the catamaran is expected to be approximately

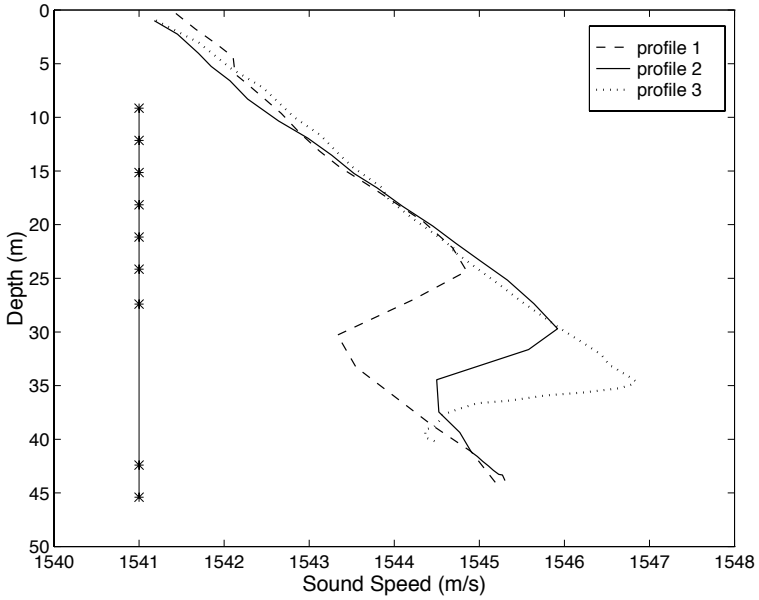

Figure 2: Three typical sound speed profiles measured at the trial site. The depths of the hydrophones used in the analysis are indicated by $*$.

100 m.

The experiment was conducted at various separations between the catamaran and the source ship of approximately 1, 7 and 12 km. The water depth over the trial interval was measured with an echosounder while the sound speed profile was monitored using a CTD probe deployed from the source ship.

The ambient noise data were collected while the VLA was drifting at the same location with the source ship approximately 20 km away. Due to the limitations of the recording length available on the analog tape, the ambient noise was recorded for approximately 5 minutes duration.

Figure 2 shows three typical profiles of the sound speed in the water column, obtained from measurement of the temperature and salinity. Over the experiment area, the depth of the thermocline varied by about 10 m.

3. Broadband Matched Field Inversion

Cast as an optimization problem, MFP includes the following[1]: an environmental model that depends on how the environment is parameterized; a forward acoustic propagation model to predict the received pressure fields based on the environmental model; a multi-frequency objective function that compares the measured and replica acoustic fields; and an efficient algorithm for searching the multi-dimensional environmental parameter space. Each of these components are described in the following paragraphs.

3.1. *Objective Function for optimization*

In the presence of noise in the environment, the spatial cross-correlation matrix of the acoustic field on the array is a more robust feature to match rather than the individual pressure variation (i.e. amplitude and phase) at the sensors[1]. We optimized the maximum-likelihood objective function[5]. It compares the measured spatial cross-correlation matrix $\mathbf{R}(\omega_l)$ of the signals on the array and the predicted replica field vectors $\mathbf{w}(\mathbf{m}, \omega_l)$ at various frequencies $\omega_l, l = 1, 2, 3, ..., L$.

$$\Phi(\mathbf{m}) = \frac{1}{L} \prod_{l=1}^{L} \left[tr\hat{\mathbf{R}}(\omega_l) - \frac{\mathbf{w}^\dagger(\mathbf{m}, \omega_l)\hat{\mathbf{R}}(\omega_l)\mathbf{w}(\mathbf{m}, \omega_l)}{\mathbf{w}^\dagger\mathbf{w}} \right] \tag{3.1}$$

$\mathbf{m}$ is the model vector which describes the environment and its elements are the parameters to be optimized.

3.2. *Data Processing for Correlation Matrix*

Out of the 14 available hydrophones on the array, 4 of these became disfunctional midway during the trial. The signal on the hydrophone closest to the water surface was clipped due to the high ambient noise levels at the surface which saturated the recorder. Only 9 hydrophones were used in the analysis and their corresponding depths are shown in Fig. 2.

At each frequency of transmission by the projector, the signal on the array was recorded for approximately 15 s. These signals were segmented into $k = 20$ blocks, each with a duration of 1.4 s. The segments overlap each other by 50%. Each segment was Fourier transformed with a resulting bin width of 1.45 Hz. The cross-correlation matrix, $\mathbf{R}$, at each tone frequency was obtained as an ensemble average over the 20 segments.

Let $\mathbf{x}_k(\omega_l)$ be the complex pressure on the array obtained from Fourier transform. Then, the cross-correlation matrix is given by

$$\hat{\mathbf{R}}(\omega_l) = \frac{1}{K} \sum_{k=1}^{K} \mathbf{x}_k(\omega_l)\mathbf{x}_k^\dagger(\omega_l). \tag{3.2}$$

Figure 3 illustrates the features of the cross-correlation matrix at 400 Hz with the receiving array at a range of about 1 km away from the source. At this frequency, the signal to noise ratio is approximately 14 dB. At a bin width of 1.45 Hz, most of the energy is contained within that band and the adjacent bins have much smaller levels.

3.3. *Selection of Data as Observation in the Optimization*

Figure 4a shows the largest eigenvalue from the eigen decomposition of the cross-correlation matrix at each frequency of transmission by the projector. Also shown is the noise floor at each frequency. The frequencies higher than 800 Hz have very good signal to noise ratio. For frequencies below 350 Hz, the noise and signal levels are equivalent. Data below 350 Hz was not used in the objective function due to the poor signal to noise ratio. Only data measured by the VLA with the source ship approximately 1 km away was considered. Data at this range had the highest signal level.

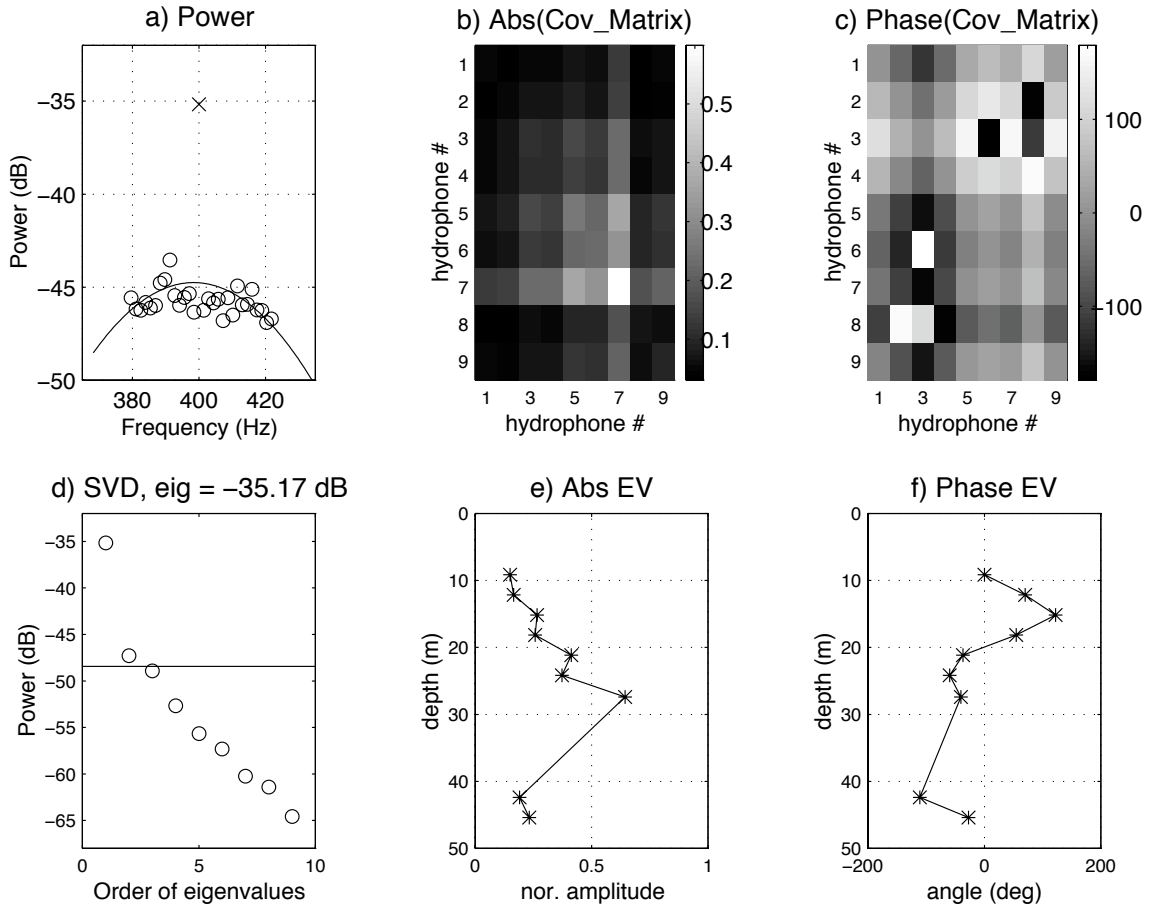

Figure 3: Analysis of a received signal. This is used for selecting the frequencies and for quality control of the data. First the cross-correlation matrix is formed for several bins in a selected frequency interval. Based on the first eigenvalue of the cross-correlation matrix at each bin (a) the frequency with the highest power is selected [marked with a cross], the corresponding magnitude (b) and phase (c) of the this correlation matrix is plotted. All the eigenvalues for this cross-correlation matrix (d) is then plotted; the estimated noise floor (solid line) is from a source-free section of the time series. The SNR is seen to be about 14 dB. Based on the cross-correlation matrix, magnitude (e) and phase (f) of the first eigenvector is plotted. Figure 3e can be used for detecting unusual gain for a hydrophone and Fig. 3f can be used to detect a 180° phase shift of the signal on a receiver.

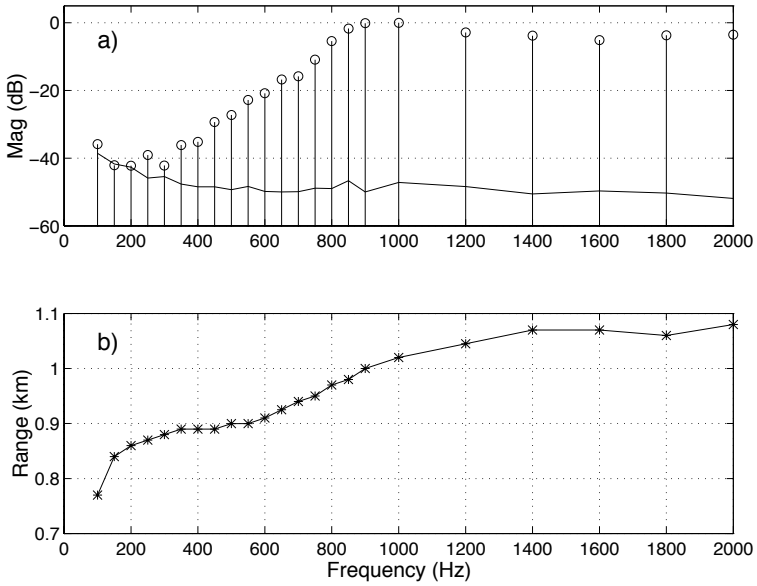

Figure 4: a) The largest eigenvalues at each frequency. The largest eigenvalue is normalized to 0 dB. There is no correction for the source spectrum. The fall-off below 900 Hz is due to limited source power at these frequencies. The noise floor (full line) is found from a signal-free time series. b) The source receiver range based on GPS readings.

As both the catamaran holding the VLA and the source ship were drifting during the measurement, the range separation between them varied for different frequencies of transmission by the projector. Figure 4b shows the range separation at each frequency based on the GPS measurement of the source ship and catamaran location. The range variation is smallest when the source frequency is between 350 to 600 Hz and between 1.4 to 2 kHz.

In order to combine the data of various frequencies in the objective function, they have to be measured at the same fixed range from the source. Otherwise, different ranges would have to be optimized for each frequency. With a source at 990 m from the array for the baseline environment (described in Sec. 3.4), Fig. 5 shows the variation in the *Bartlett power measure*[12] with range at various frequencies. At lower frequencies, around 300 Hz, measurements with range differences of up to 80 m may be combined. At higher frequencies, the range variation of the measured data has to be much smaller. Data with frequencies from 350 to 600 Hz and 1.4 to 2 kHz were used separately in the inversion. The bin width for each frequency was 1.45 Hz.

3.4. *Parameterization of the Environment*

As the frequencies used in the inversion were relatively high (>300 Hz), the depth of penetration of the acoustic wavefield into the sea bottom is expected to be small due to attenuation. Therefore the properties of the sea bottom close to the water-sediment interface are the important ones for high frequencies. The environmental model was assumed to

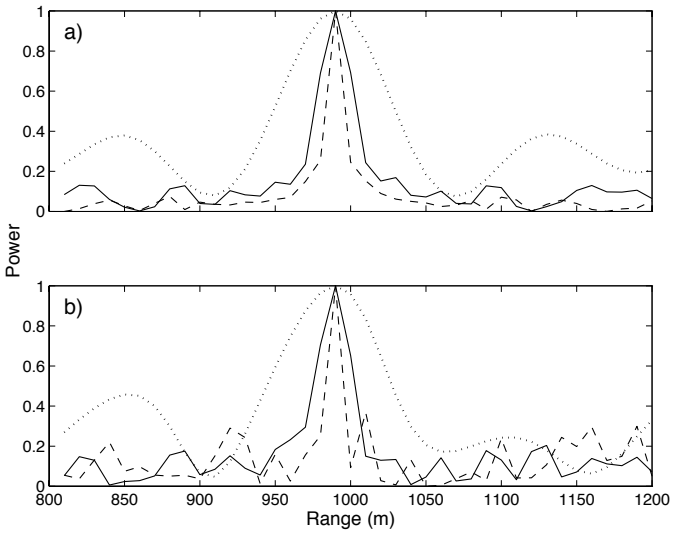

Figure 5: The variation in Bartlett power for the baseline environment using (a) an array covering the whole water column and (b) the sparse array used here. The frequencies are 300 Hz (dotted line), 1000 Hz (full line), and 2000 Hz (dashed line). The source is assumed to be at a range of 990 m. For the higher frequencies the peak is much narrower; this makes localization across frequencies more difficult.

be range independent, consisting of a water layer overlying a sediment halfspace. The properties of the sediment halfspace obtained from inversion would correspond to the sea bottom properties close to the water-sediment interface.

For the purpose of inversion, the forward model parameters to be optimized were subdivided into three subsets; geometric, water and sediment. The geometric parameters include range and depth of the source, and tilt and depth of the receiver array. The water depth was also optimized. The sediment properties include compressional speed, attenuation and density. As the source was not placed too close to the sea floor, shear (even if it were present) is not expected to affect the acoustic field pattern in the water column. Hence, shear in the bottom was neglected. The water sound speed profile varies at the measurement site as shown in Fig. 2. Each of these profiles was used separately in the inversion. The forward model used to generate the replica acoustic field is SNAP[13], a normal mode propagation model.

3.5. *GA Optimization and A Posteriori Analysis*

The SAGA[14,4] code, based on genetic algorithms (GA) as the search method, was used for searching the model parameter space to obtain the parameter values that yield the best match to the data. The GA search parameters were selected as follows. The population size was set to 64, the reproduction size was 0.5, the crossover probability was 0.8 and the mutation probability was 0.05. The GA search was advanced for 10 independent populations

Model Parameters	Lower Bound	Upper Bound
Geometric:		
Source range (m)	800	1200
Source depth (m)	12	15.5
Receiver depth (m)	8	10.5
Array tilt (m)	-6	6
Water:		
Water depth (m)	49	52
Sediment:		
Sound Speed (m/s)	1548	1700
Attenuation (dB/λ)	0.01	1

Table 1: GA inversion model with parameter search bounds. The search space for each parameter was discretized into 128 values.

and the number of iterations was restricted to 2000 per population. Hence, a total of 2×10^4 forward model runs was performed for each signal realization (number of iterations $\times$ the number of independent populations).

After each inversion, 320 candidate solutions of the model vector $\mathbf{m}$ were saved to analyze the convergence of the algorithm (population size $\times$ reproduction size $\times$ number of independent populations). These solutions were weighted with their fitness before constructing the *a posteriori* distributions.

3.6. *Low frequency Inversion Result*

Optimization was carried out using the low frequencies from 350 to 600 Hz to estimate the 7 unknown parameters (see Table 1). The receiver depth refers to the depth of the shallowest hydrophone. The GA uses this parameter to optimize the vertical position of the entire array in the water column. The array tilt refers to the horizontal deviation at the last receiver. Table 1 provides the search bounds for each parameter. For an array of 40 m in length, a horizontal deviation of about 6 m in the last receiver corresponds to an angular tilt of about 9°. For each parameter, the search space was quantized into 128 increments. For seven parameters with a quantization of 128 steps, we have a search space of 10^{14} samples. However, only 20000 models were computed. Thus, only a small fraction of the search space was sampled. Each of the three sound speed profiles in Fig. 2 were used in separate inversion runs. Each inversion required a minimum of 1000 s of CPU time on an AlphaStation model 500, 500 MHz workstation.

Figure 6 shows the *a posteriori* distribution[4,15] of the estimates obtained using Profile *2* of the water column sound speed profiles in Fig. 2. The *a posteriori* distribution indicates the variability of the parameter estimates over the search interval. It is seen that the source range and depth, compressional speed of the sediment and the array tilt are quite

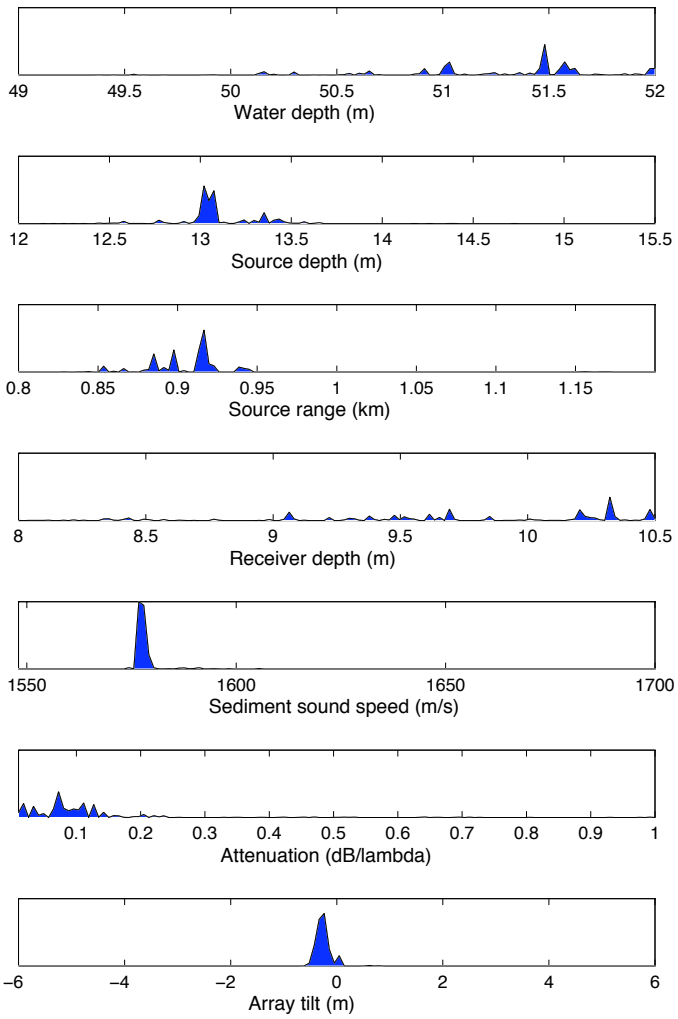

Figure 6: Probability distribution for environment with water column sound speed profile *2* using the 350 to 600 Hz data.

Parameter		Estimated values			
		Best Fit	Max ppd	Mean ppd	nor. sd
Geometric:					
Source range	(m)	916	916	907	0.07
Source depth	(m)	13.0	13.0	13.1	0.07
Receiver depth	(m)	9.9	10.3	9.7	0.25
Array tilt	(m)	-0.24	0.24	0.26	0.013
Water:					
Water depth	(m)	51.6	51.5	51.3	0.16
Sediment:					
Sound Speed	(m/s)	1578	1577	1578	0.02
Attenuation	(dB/λ)	0.03	0.07	0.1	0.12

Table 2: Estimated parameters for environment with Profile *2* using the three estimation methods.

well determined. Their distributions are compact over the search interval and there is an unambiguous peak indicating that the inversion was fairly successful at finding a good fit for these parameters. The remaining parameters are not as well determined.

Based on the *a posteriori* distribution over the search interval, three possible estimates of the unknown parameters may be obtained.

- Best fit - the model vector (parameter set) with the best fit to the data during the optimization.
- Max ppd - the maximum of each marginal *a posteriori* probability distribution.
- Mean ppd - the mean of each marginal *a posteriori* probability distribution.

When there is little difference between the three estimates it indicates that a reliable solution has been obtained. The value of the three estimates based on the *a posteriori* distribution for Profile *2* is shown in Table 2. Also shown is the normalized standard deviation of each parameter which is the standard deviation of the parameter value, scaled by the length of the search interval. This describes how well the estimates are clustered within the search interval. A peaky distribution for the parameter leads to a small value for the normalized standard deviation which indicates that the parameter is important in acoustic propagation. A large and scattered distribution on the other hand leads to a large value for its standard deviation which implies that the parameter is less important in the propagation of the acoustic wavefield. The source range and depth, sediment sound speed and array tilt have small normalized standard deviations indicating that these have been well estimated.

Figure 7 shows the normalised magnitude of the pressure field measured across the array and the *Bartlett power measure* of the modelled field from the best fit parameters.

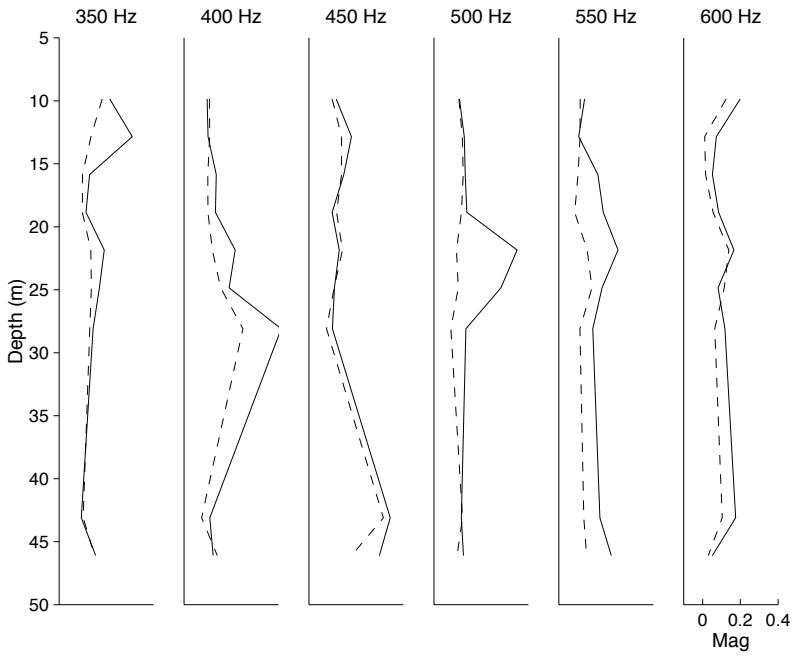

Figure 7: The best global match obtained using Profile *2*. The solid curve is the normalized magnitude of the measured field and the dashed curve is the corresponding *Bartlett power measure* obtained with the modelled field.

The *Bartlett power measure*[12] can be interpreted as the degree of phase matching between the measured data and modelled replica at each phone weighted by the magnitude of the pressure field. Thus, it contains more information than plotting the magnitude of the pressure alone. Bearing in mind the fact that the data set being matched is from a real measurement, the match obtained is quite good at most of the frequencies.

With regard to the estimates obtained using the various water column sound speed profiles, Table 3 shows the parameter values giving the best match to the data. The estimates for the sediment sound speed are almost identical indicating reliable estimation. The estimates of the source range and array tilt are also very close. A horizontal deviation of about 0.5 m corresponds to an angular tilt for the array of 0.7°. Despite the variation in the depth of the sound speed maximum in the water column, the estimates obtained for the various parameters are stable. This indicates that inversion at these frequencies is robust with regard to changes in the sound speed profile in the water column.

When the layering of the sediment is included in the inversion, very similar results to the above estimates were obtained. The environment was assumed to consist of a single sediment layer overlying a bottom half space. The inversion indicated a sediment thickness of 1.2 m with a compressional speed varying from 1565 m/s at the top of the sediment to 1575 m/s at the bottom of the sediment layer. The bottom half space beneath the sediment layer was linked to the bottom of the sediment layer. These results are consistent with our

Parameter		Estimated Best fit values		
		Profile *1*	Profile *2*	Profile *3*
Source range	(m)	913	916	894
Source depth	(m)	13.3	13.0	13.0
Array tilt	(m)	-0.6	-0.2	-0.2
Sediment Sound Speed	(m/s)	1577	1578	1577

Table 3: The best fit estimate for several well determined parameters (with small normalized standard deviations), for three different water sound speed profile when using the 350 to 600 Hz data.

assumption that the seafloor properties are more important than the deeper layers of the bottom as relatively high frequencies (>300 Hz) were used in the inversion.

3.7. *High frequency Inversion Result*

The high frequency data from 1.4 to 2.0 kHz were used to optimize the same seven parameters as indicated in Table 1 in separate runs using the different sound speed profiles in the water column. The high frequency inversion was found to be unstable. The estimates obtained for the various parameters were inconsistent with each other in all three runs. Moreover, some of the parameters, e.g. the source range, where we had *a priori* information were estimated to be at the bounds of the search interval indicating an incorrect solution. This implies that high frequency inversion is very sensitive to the sound speed profile in the water column.

We therefore decided to invert for the sound speed profile in the water column. Upon closer examination of the three profiles, it is evident that these profiles have essentially the same slope. They differ however, in the depth of the thermocline. The problem was parameterized to include this depth, d, as an unknown in the inversion. The sound speed profile was modelled using three piece-wise linear shape functions[5]. The sound speeds, $c(z)$ (in m/s), at the various depths, z (in m), are given by

$$\begin{aligned} c(0) &= 1541 \\ c(d) &= c(0) + S{\times}d \\ c(d+5.5) &= c(d) - 1.5 \\ c(50) &= c(0) - 1.5 + S{\times}(50 - 5.5), \end{aligned} \tag{3.3}$$

where S is the slope of the profile which measures the change in the sound speed with depth (see Fig. 8). The deficit in sound speed below the thermocline for all profiles is close to 1.5 m/s and decays over 5.5 m. The search interval for the thermocline depth d, was set to lie between 20 to 35 m.

Figure 9 shows the *a posteriori* distribution[4,15] of the estimates for the inversion using high frequency data. Table 4 shows the statistics of the distribution for some of the param-

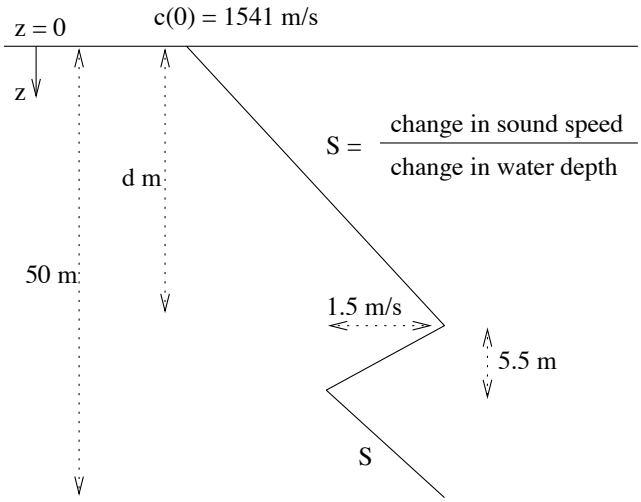

Figure 8: Sound speed profile in the water column modelled by shape functions.

Parameter		Estimated values			
		Best Fit	Max ppd	Mean ppd	nor. sd
Geometric:					
Thermocline depth, d	(m)	24.7	25.2	25.0	0.05
Source range	(km)	1.14	1.14	1.11	0.15
Source depth	(m)	14.0	14.0	13.9	0.08
Array tilt	(m)	3.3	3.3	3.3	0.007
Sediment Sound Speed	(m/s)	1564	1548	1553	0.04

Table 4: Estimated parameters with the optimization of the thermocline depth at high frequencies.

eters. The distribution for the thermocline depth is compact and has a well defined peak at about 25 m. This thermocline depth corresponds to Profile *1* of the measured sound speed profiles in Fig. 2. The estimates for the source range and depth are now well within the search bounds. The current at the trial site was about 1 m/s. Over the measurement period for frequencies from 1.4 to 2 kHz, the scatter in the *a posteriori* distribution for the source range is comparable to the range variation due to the drift of the source ship.

The low frequency and high frequency inversion results cannot be directly compared, as the measured data were separated in time by 20 min and the range was approximately 20% larger at the higher frequencies. Also the low and high frequency inversions have different sensitivities. It is also possible that all the relevant physical phenomena have not been modelled at the high frequencies. The array tilt could in principle vary with time. However, a variation of 3 m seems quite large. The estimate for the depth of the first receiver appears to be at the lower bound of 8 m. It not likely for the depth to be shallower than 8 m as the physical depth of the corresponding hydrophone is 9.5 m.

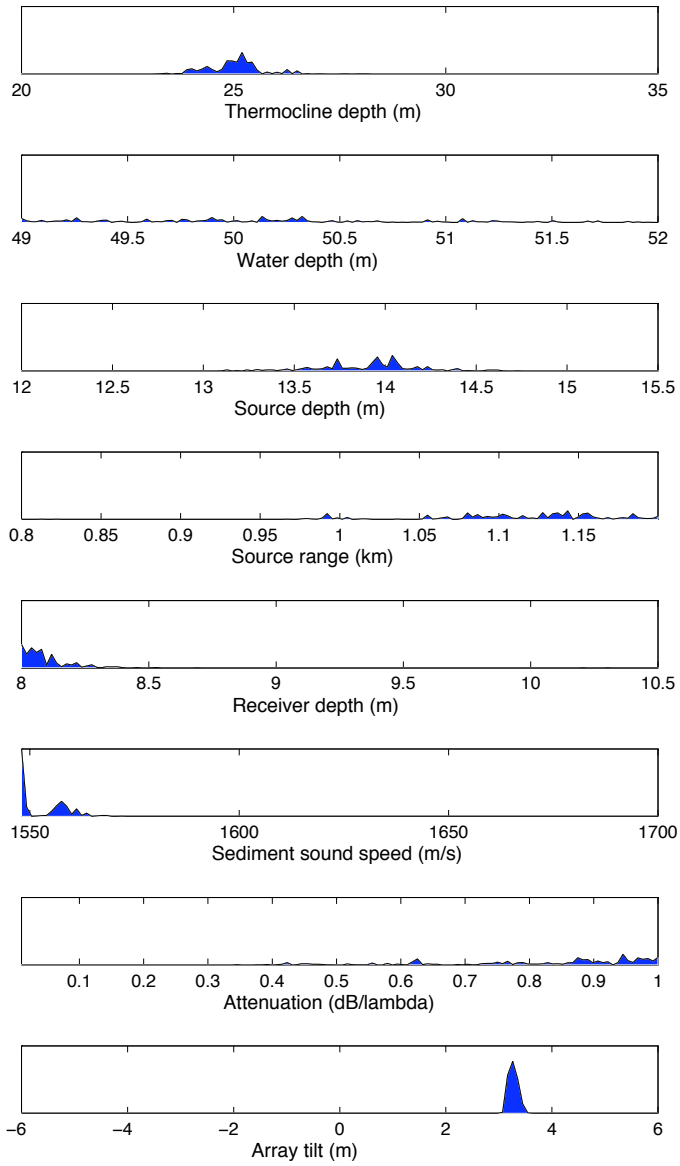

Figure 9: Probability distribution for the high frequency inversion that optimizes the depth of the thermocline.

There is more variability in the estimates of the compressional sound speed of the sea floor in the high frequency inversion in comparison to the low frequency estimates. Also, the estimated sea floor sound speed is much lower for the high frequencies. This is probably due to the fact that high frequencies are strongly affected by the sound speed profile in the water column and they have negligible penetration into the bottom. They skim the sea floor where the sediment is saturated with water and therefore detect a smaller sound speed, intermediate between that of the water column and the sediment.

4. Ambient Noise Inversion

4.1. *Ambient Noise in Shallow Water*

The ambient noise inversion approach that we adopt follows closely that of Buckingham and Jones[11]. As noise propagates through a shallow water channel, it interacts with the channel boundaries and acquires characteristics that are related to the physical properties of the transmission path i.e. the medium itself, the sea surface and the seabed. In a shallow water medium with a fast lossless fluid bottom (i.e. a Pekeris channel), one feature of the ambient noise that is strongly controlled by the bottom interface is the distribution of the noise field in the vertical. For such a medium, the water-sea bottom interface shows a critical grazing angle α_c. Rays that approach the interface with grazing angles less than α_c are totally internally reflected, while rays with grazing angles greater than α_c are heavily attenuated due to penetration into the bottom. Therefore the totally internally reflected rays propagate large distances through the channel and give rise to a strong concentration of noise around the horizontal that extends to an angular region α_c on either side of the horizontal. For local wind-driven sources of noise, their contribution to the overall noise field is approximately isotropic. Figure 10 shows a sketch[11] of the vertical distribution of the ambient noise expected in a shallow water environment where a and b are the amplitudes of the noise field due to the distant (e.g. wind or distant shipping) and local wind-driven sources of noise respectively.

Changes in the surface condition in such an environment would significantly alter the noise levels, a and b, but the angular width of the noise distribution in the vertical due to the long range sources would be invariant.

4.2. *Spatial Coherence of the Noise*

For two vertically displaced sensors in such a medium, the coherence of the noise fluctuation at the two sensors is given by[11]

$$\Gamma_{sw}(\Omega) = \frac{b}{\Omega}\sin(\Omega) + \frac{1-b}{\Omega\sin(\alpha_c)}\sin[\Omega\sin(\alpha_c)]. \tag{4.4}$$

Ω is a dimensionless quantity that is related to the noise frequency, f, the sound speed in the water column, c_1, and the separation between the two sensors, l,

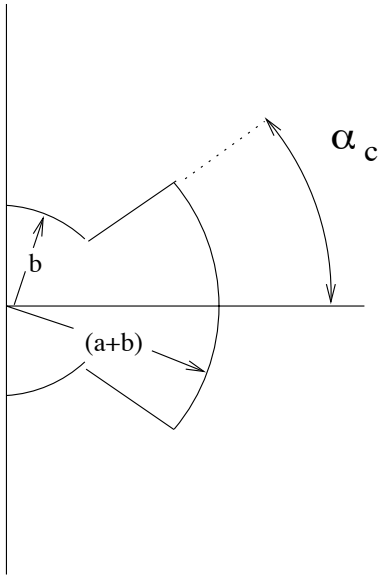

Figure 10: Model of the vertical distribution of ambient noise in a Pekeris wave-guide.

$$\Omega = \frac{2\pi f l}{c_1}. \tag{4.5}$$

When the two sensors are coincident (i.e. when Ω is zero), $\Gamma_{\rm sw}$ is unity as the noise is fully correlated. When the sensors are many wavelengths apart (i.e. when Ω goes to infinity), $\Gamma_{\rm sw}$ goes to zero and the noise is uncorrelated. The theoretical model predicts that the coherence of the noise at the two sensors is real due to symmetry of the noise field about the horizontal. For an asymmetrical noise distribution in the vertical the coherence function is complex with a large imaginary component. The above model of the ambient noise assumes that there is no local shipping in the area around the receivers as this would distort the shape of the noise field significantly. Other assumptions made by the model are that the bottom is fluid, i.e. the shear properties are negligibly small or absent, and that the P-attenuation of the bottom is also small.

4.3. *Optimization Strategy to determine Bottom Speed*

By experimentally measuring the coherence between two vertically displaced sensors in the shallow water channel, $\alpha_{\rm c}$ the critical grazing angle of the water-bottom interface may be found by comparison with Eq. (4.4) at a number of frequencies. The compressional speed of the bottom c_2 can be derived from $\alpha_{\rm c}$ using Snell's law,

$$c_2 = \frac{c_1}{\cos(\alpha_{\rm c})}. \tag{4.6}$$

As there are only two unknowns b and $\alpha_{\rm c}$ in Eq. (4.4), they can be easily determined by implementing an optimization procedure that searches for these two unknowns. The

objective function to be optimized provides a least squares fit between the measured coherence function, Γ_{meas}, and the real-valued theoretical coherence function, Γ_{sw}. By taking the reciprocal of this fit, we cast it as a maximization problem.

Maximize:

$$\Phi_{\text{ls}} = \left[\frac{1}{N} \sum_{n=1}^{N} \left| \Gamma_{\text{sw}}(\Omega_n, b, \alpha_{\text{c}}) - \text{Real}\{\mathbf{\Gamma}_{\text{meas}}(\Omega_n)\} \right|^2 \right]^{-1}, \tag{4.7}$$

subject to the constraints:

$$0.05 < b < 1.0, \tag{4.8}$$

$$0.05 < \alpha_{\text{c}} < 1.5. \tag{4.9}$$

In the above formulation, Ω_n are the discrete frequencies at which the ambient noise is used in the inversion. As b represents noise power, it is a positive quantity and the normalization condition[11] imposed on the vertical distribution of the noise power sets it's upper limit to 1.

4.4. *Ambient Noise Inversion Result*

Approximately 300 s (5 min) of the ambient noise data were segmented into 200 blocks with 50 % overlap. The ambient noise spectrum was obtained as an ensemble average over the individual spectrum computed for each segment. The resulting frequency bin width was 1 Hz. The spectrums of the ambient noise measured by the two hydrophones in the middle of the water column are shown in Fig. 11. The ambient noise spectrums are smoothly varying from low frequencies up to 800 Hz. Beyond 800 Hz, there are some peaks in the spectrums probably due to nearby shipping which tends to distort the vertical distribution of the noise field. Therefore in the inversion, the ambient noise data used was restricted to below 800 Hz.

Figure 12 shows the real and imaginary component of the coherence between the two hydrophones which have a separation of 3 m. The imaginary component of the coherence is very small. This indicates that the ambient noise field at the trial site for frequencies below 800 Hz has a symmetrical distribution in the vertical direction and the data are suitable for inversion by the method outlined above.

A MATLAB code to do the optimization required only a minute of computation time on a Pentium Pro 200 MHz PC. Figure 13 shows the ambiguity surface for the optimization of the two parameters b and α_{c} using the measured coherence between the two hydrophones in the objective function. The objective function value for various combinations of b and α_{c} has been normalized by its peak value which occurs at $b = 0.58$ and $\alpha_{\text{c}} = 0.22$ rad. Using a sound speed in the water (close to the seafloor) of 1545.7 m/s, the sound speed of the sediment was obtained from Snell's law to be 1584 m/s. Also shown in Fig. 13 are the contour lines corresponding to the objective function having 90% and 70% of it's peak value. At 90% of the peak value, the sound speed estimate for the sediment ranges from 1550 m/s to 1610 m/s. Figure 12 shows the fit between the theoretical and measured coherence. The trend of the measured coherence is well approximated by the theoretical coherence.

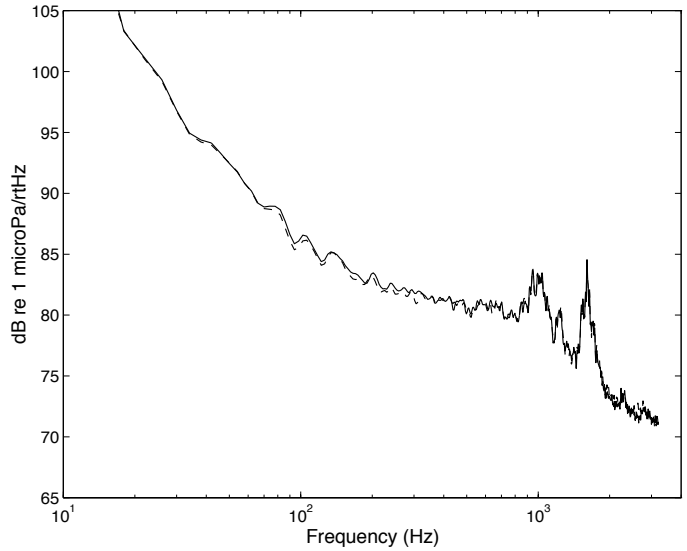

Figure 11: Spectrum of the ambient noise on two hydrophones in the middle of the water column at the depths of 21 m (solid line) and 24 m (dashed line) respectively.

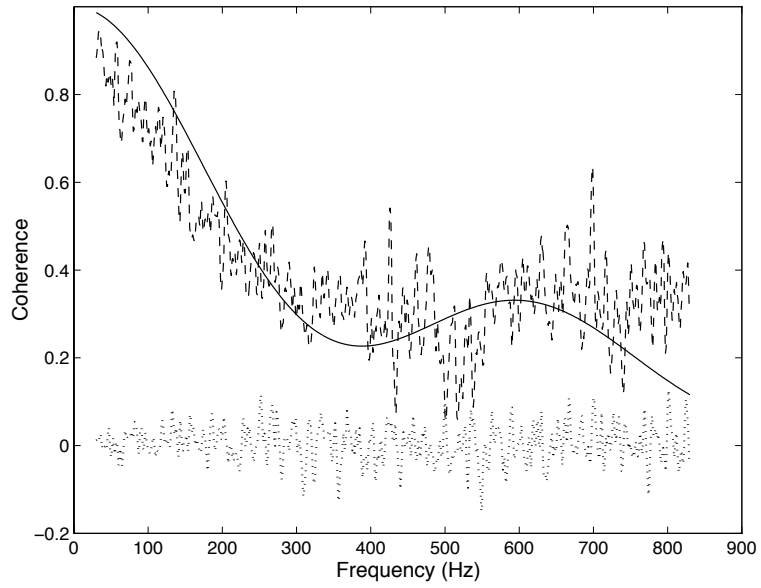

Figure 12: Coherence of the measured ambient noise between the two hydrophones; real component (dashed curve) and imaginary component (dotted curve). The theoretical coherence obtained from the model (solid line) shows a good fit to the trend of the real component of the observed coherence.

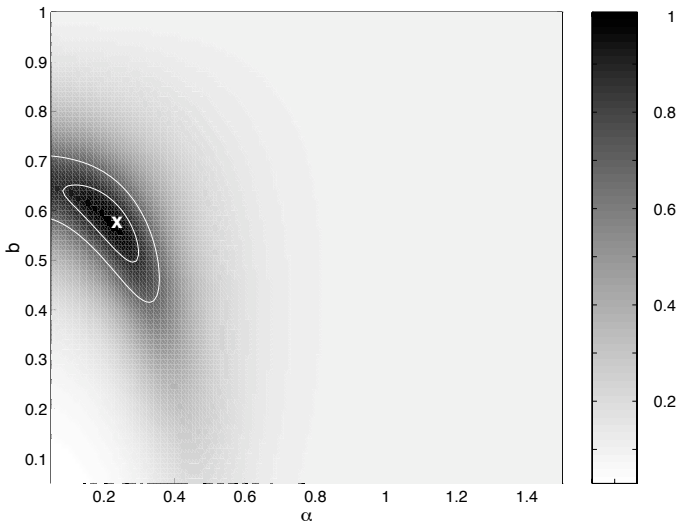

Figure 13: Normalized ambiguity surface for the optimization with two parameters, b and α_c. The maximum is marked by $\times$ which corresponds to $b = 0.58$ and $\alpha_c = 0.22$ rad.

Method	Sediment Sound Speed (m/s)
MFP	1577
ANI	1584
Historical	1570

Table 5: Estimated sound speed of the sediment obtained from MFP and ANI is compared to historical data.

5. Comparison of Estimated Sediment Properties

Table 5 lists the estimated properties of the sea floor obtained from ANI and MFP. The sound speed of the sediment estimated by the two approaches are very close. According to historical records of the trial site, the sea bottom comprises of a muddy sediment layer of thickness between 20 to 90 m overlying a rock basement. The estimated compressional speed of the seafloor obtained from inversion compares well with that of mud provided in the historical records of 1570 m/s.

6. Discussions

Both low and high frequency data have been inverted via MFP to deduce the properties of the environment. Inversion estimates using low frequencies were found to be more robust to variations in the environment. At high frequencies, the estimates were much affected by fluctuation in the environment, for e.g. the thermocline depth. We have used shape functions to re-parameterize the environment to obtain more stable and meaningful results. The concept of shape function is particularly useful in practical data collection schemes

where the measured data tend to have more temporal and spatial variation due to the use of less sophisticated instrumentation in the data collection. Shape functions provide us with the ability to represent an aggregate effect of the environment from the observed data.

The properties of the sea floor deduced from inversion by MFP agree well with the results obtained from ANI and also with historical data. ANI is a useful technique for rapid environmental assessment due to the fact that it can be easily implemented. At present, we have worked with data from a single pair of sensors. Further work is necessary to examine the effects of using data from sensors with different separation. Also, the technique can be extended to include shear effects[16,17] of the environment.

It seems clear that broadband matched field inversion contains more information about the environment than ambient noise inversion, both in terms of accuracy and the number of parameters. However, the latter is considerably simpler.

References

1. A. Tolstoy *Matched Field Processing for Underwater Acoustics*, (World Scientific, NJ., 1993).
2. A.B. Baggeroer, W.A. Kuperman, and Mikahalevsky, "An overview on matched field methods in ocean acoustics", IEEE J. Oceanic. Eng. **18** (1993).
3. M. Collins and B. Kuperman and H. Schmidt, "Nonlinear inversion for ocean bottom properties," J. Acoust. Soc. Am. **92**, 2770–2783 (1992).
4. P. Gerstoft, "Inversion of seismo-acoustic data using genetic algorithms and *a posteriori* probability distributions," J. Acoust. Soc. Am. **95**, 770–782 (1994).
5. J-P. Hermand and P. Gerstoft, "Inversion of Broadband multitone acoustic data from the Yellow shark summer experiments," IEEE Oceanic Eng. **21**, 324–346 (1996).
6. Z-H. Michalopoulou and M.B. Porter and J.P. Ianniello, "Broadband source localization in the Gulf of Mexico," J. of Computational Acoustics **4**, 361–370 (1996).
7. N.R. Chapman, K.S. Ozard, and C.A. Zala, "Matched field inversion using an adaptive global search algorithm," 3rd European Conference on Underwater Acoustics, Crete University Press, Heraklion, Crete, Greece. 335–340 (1996).
8. N.R. Chapman and C.E. Lindsay, "Matched-Field Inversion for Geoacoustic Model Parameters in Shallow Water," IEEE Oceanic Eng. **21**, 347–354 (1996).
9. C.E. Lindsay and N.R. Chapman, "Matched field inversion for geophysical parameters using adaptive simulated annealing," IEEE J. Oceanic Eng. **18**, 224–231 (1993).
10. E.L. Hamilton, "Geoacoustic modelling of the sea floor," J. Acoust. Soc. Am. **68**, 1313–1339 (1980).
11. M.J. Buckingham and S.A.S. Jones, "A new shallow water technique for determining critical angle of the seabed from the vertical directionality of the ambient noise in the water column," J. Acoust. Soc. Am. **81**, 938–946 (1987).
12. P. Gerstoft and D.F. Gingras, "Parameter estimation using multi-frequency range-dependent acoustic data in shallow water," J. Acoust. Soc. Am. **99**, 2839–2850 (1996).
13. F.B. Jensen and M.C. Ferla, "SNAP-The SACLANTCEN normal mode acoustic propagation model," SACLANT Undersea Research Centre, SM–121, La Spezia, Italy (1979).
14. P. Gerstoft,"SAGA Users guide 2.0, an inversion sofware package," SACLANT Undersea Research Centre, SM–333, La Spezia, Italy (1997).
15. D.F. Gingras and P. Gerstoft, "Inversion for geometric and geoacoustic parameters in shallow water: Experimental results," J. Acoust. Soc. Am. **97**, 3589–3598 (1995).
16. M.J. Buckingham, G.B. Deane, and N.M. Carbone, "Inverting ambient noise in shallow water for the bottom geo-acoustic parameters," in Full Field Inversion Methods in Ocean and Seismo-

Acoustics, Kluwer Academic Publishers, Dordrecht, the Netherlands. 347–352 (1995).
17. N.C. Carbone, G.B. Deane, and M.J. Buckingham, "Estimating the compressional and shear wave speed of a shallow water seabed from the vertical coherence of ambient noise in the water column," to appear in J. Acoust. Soc. Am. (1997).